

Effect of hopper angle on granular cloggingDiego López-Rodríguez,¹ Diego Gella,¹ Kiwing To,² Diego Maza,¹ Angel Garcimartín,¹ and Iker Zuriguel^{1,*}¹*Departamento de Física, Facultad de Ciencias, Universidad de Navarra, E-31080 Pamplona, Spain*²*Institute of Physics, Academia Sinica, Taipei 115, Taiwan.*

(Received 31 October 2018; published 8 March 2019)

We present experimental results of the effect of the hopper angle on the clogging of grains discharged from a two-dimensional silo under gravity action. We observe that the probability of clogging can be reduced by three orders of magnitude by increasing the hopper angle. In addition, we find that for very large hopper angles, the avalanche size ($\langle s \rangle$) grows with the outlet size (D) stepwise, in contrast to the case of a flat-bottom silo for which $\langle s \rangle$ grows smoothly with D . This surprising effect is originated from the static equilibrium requirement imposed by the hopper geometry to the arch that arrests the flow. The hopper angle sets the bounds of the possible angles of the vectors connecting consecutive beads in the arch. As a consequence, only a small and specific portion of the arches that jam a flat-bottom silo can survive in hoppers.

DOI: [10.1103/PhysRevE.99.032901](https://doi.org/10.1103/PhysRevE.99.032901)**I. INTRODUCTION**

The flow of systems composed by discrete particles is intrinsically complex yet several constitutive relations have been proved to describe it rather accurately. Nevertheless, when the particles are strongly confined and the boundaries effect becomes dominant, the problem turns out to be extremely complicated and our understanding about it is very limited. An example of this instance is the phenomenon of clogging in bottlenecks, which can be seen as a sudden transition from a flowing state to an arrested state caused by the formation of a structure near the neck that stops the flow.

In active systems, clogs might be shattered by the internal energy of the particles, then leading to an intermittent flow as in the case of active grains [1], sheep flocks [2], or pedestrian crowds [3,4]. This intermittency can also be found in systems of passive elements such as microparticles [5–8], droplets [9,10], or even granular matter [11], where external perturbations (such as pressure gradients or vibrations) trigger the recovery of the flow. Nevertheless, for the case of inert grains in a silo, if no external perturbation is applied, a clogging arch would persist forever [12–17]. For this reason, despite its apparent simplicity, static silo configurations are ideal to study the process of clogging.

Among the works dealing with the silo clogging problem, only a few have detected that the hopper angle has some influence [12,18–20], but the role of this parameter has never been systematically studied. Yet, given the influence of the hopper angle on the silo flow properties [21–25] and the intriguing avalanche distributions documented for anisometric wedge hoppers [26], it seems reasonable to investigate the way in which clogging is affected by the hopper angle.

In this work, we experimentally analyze the effect of the hopper angle in the clogging process of inert grains discharged

from a silo. Surprisingly, we find a strong dependence of clogging probability on this parameter that, to our knowledge, has gone ignored in previous studies. From our detailed analysis of the arch properties, an explanation of this dependence is provided based on geometrical arguments.

II. THE EXPERIMENT

The experimental setup is similar to the silo implemented in [27,28] except that three other hopper-like geometries (see Fig. 1) have been used besides the flat bottom silo. The silo, which was built in a quasi-two-dimensional fashion, consists of two 10 mm thick parallel glass sheets. The walls and bottom are 1 mm thick movable stainless steel pieces sandwiched between the glasses. These pieces have been supplemented with thin aluminum foil tape in such a way that the particles, AISI 420 stainless steel spheres of $d = 1$ mm diameter, fit inside the reservoir and arrange in a single layer. The shape and position of the lateral and bottom walls determine the silo size (which is always 750 mm high and 280 mm wide) and the bottleneck geometry. The latter is characterized by β , the angle between the horizontal and the hopper bottom (see Fig. 1). In this work, four different values of β have been investigated. The other explored parameter is the outlet size D , the length of the narrowest passage position along the neck as illustrated in Fig. 1. Note that the geometry of the bottleneck is designed in such a way that the width increases below the orifice (the narrowest point in the neck), hence preventing the emergence of clogs along the outlet. In previous works, we checked that these clogs were rare, but possible, if the neck was straight. The experimental setup is complemented with a top hopper to fill the silo; a bucket on a balance to gather the material and register the mass of each avalanche; a camera and a rear LED panel to take high contrast pictures of the arches; and an air blower placed below the orifice to unclog the system.

*iker@unav.es

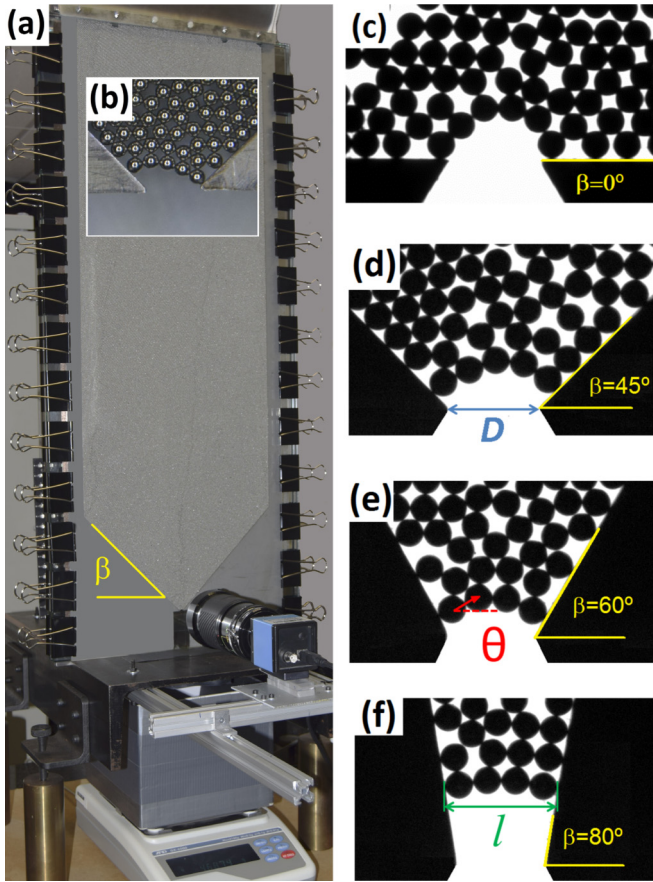


FIG. 1. (a) Photograph of the experimental setup with (b) a zoom of the outlet region. Also we show four typical arches formed in (c) a flat-bottom silo ($\beta = 0^\circ$); (d) a hopper with $\beta = 45^\circ$; (e) a hopper with $\beta = 60^\circ$; and (f) a hopper with $\beta = 80^\circ$.

The experimental procedure is as follows. First the silo is filled from the top and we wait until an arch clogs the outlet. Next, the balance is tared. Then, the blower is turned on during half second and the air jet destroys the arch, hence restarting the flow. When a new arch eventually clogs the system again, the event is detected by the balance as the readout suddenly stops increasing. Then, the avalanche weight is obtained and converted to avalanche size s (in number of grains) using the weight of a single particle. Finally, the camera takes a photograph of the arch, and the blower triggers a new avalanche. This automated process is monitored with a PC and can be repeated as many times as required; typically 3000 times for each experimental condition to ensure sufficient statistics.

From the photographs taken by the camera, we identify all the particles in the arch using the image processing codes (in Matlab) developed in Ref. [28]. For the case of a flat bottom silo, only the particles belonging to the arch structure were considered, excluding those conforming the base. In particular, in this work we have computed the number of beads of each arch n , the vector angle θ among every two consecutive beads in the arch, and the arch size in the horizontal direction or arch span, l . In order to define θ , we consider the vectors joining the centers of the particles of the arch, from left to right, and we calculate the angle with respect to the horizontal. In this way, θ_1 accounts for the vector angle between the first

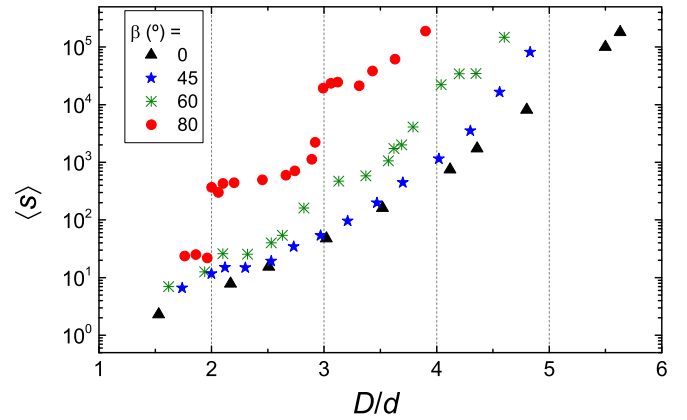


FIG. 2. Mean avalanche size $\langle s \rangle$ versus the outlet size D (rescaled by the particle size d) for different hopper angles β as indicated in the legend. The error bars, indicating the 95% confidence interval of the values obtained, are of around the symbols size. Note the logarithmic scale on the vertical axis.

and second particle (see Fig. 1), θ_2 for the angle between the second and third particle, and so on up to θ_{n-1} . The arch size is measured in the horizontal direction as this is the relevant dimension concerning clogging. In this sense, the arch span (l) is defined as the horizontal distance between the borders of the arch (Fig. 1). In practice, l is calculated as the horizontal distance between the centers of the outermost particles, plus one particle diameter.

III. RESULTS

Let us start by introducing the outcomes of the avalanche sizes for each experimental condition investigated in this work. As we know (and we have checked) that the avalanche size distribution is a decaying exponential, the mean avalanche size ($\langle s \rangle$) can be used as the parameter that characterizes it. In Fig. 2 we show $\langle s \rangle$ versus D/d (the outlet size rescaled by the particle diameter) for the four hopper angles β investigated in this work. Intriguingly, there is a qualitative difference between the outcomes for the flat-bottom silo ($\beta = 0^\circ$) and the $\beta = 80^\circ$ hopper. The flat-bottom silo exhibits a smooth dependence on $\langle s \rangle$ with D/d , while the $\beta = 80^\circ$ hopper displays a growth in steps. Quantitatively, the introduction of the hopper geometry leads to an increase of the mean avalanche size that is rather small for $\beta = 45^\circ$, but becomes more pronounced as the hopper angle grows. Also, it can be observed that the differences among the curves increase with the outlet size, reaching almost three orders of magnitude (from $\langle s \rangle \approx 10^2$ to $\langle s \rangle \approx 10^5$) between the flat-bottom silo and the $\beta = 80^\circ$ hopper when $D/d \approx 4$.

Aiming for a better understanding of these interesting features, we investigated the properties of the clogging arches. We started by looking at the number of beads conforming the arches. In Fig. 3(a) we report the average number of beads $\langle n \rangle$ of all the clogging arches obtained for every experimental condition. Remarkably, whereas for $\beta = 0^\circ$ the growth of $\langle n \rangle$ is smooth, the dependence becomes more discretized as β increases. Indeed, for $\beta = 80^\circ$ the average number of beads is $\langle n \rangle \approx 2$ for $D/d < 2$, $\langle n \rangle \approx 3$ for $2 < D/d < 3$, and

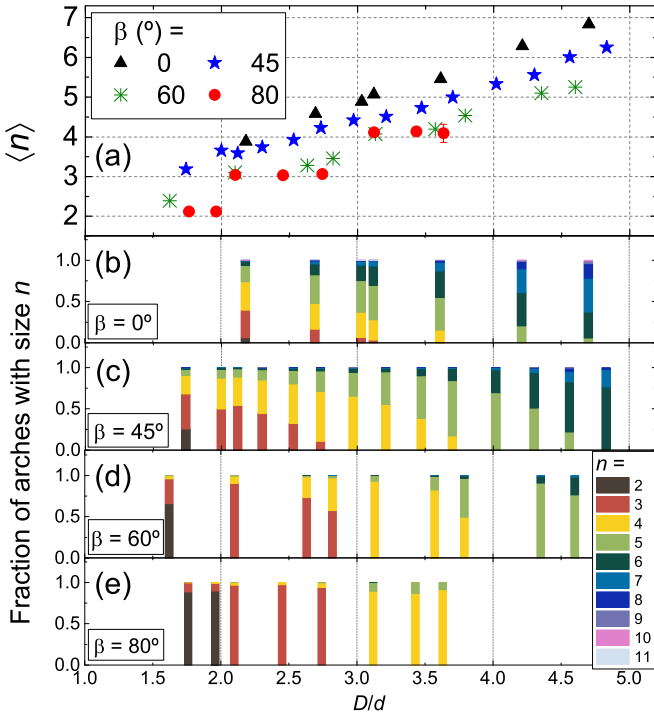


FIG. 3. (a) Average number of particles that form the arches depending on the outlet-to-particle diameter ratio D/d for the four values of β explored in this work as indicated in the legend. The error bars, indicating the 95% confidence interval of the values obtained, are of around the symbols size. (b)–(e) Bar diagrams illustrating the percentage of clogging arches formed by n beads for each experimental condition. The colors correspond to different values of n , as indicated in the legend.

$\langle n \rangle \approx 4$ for $3 < D/d < 4$. For $\beta = 60^\circ$ a reminiscence of this discretization is observed; a feature that is virtually lost for $\beta = 45^\circ$. Going a step further, we have calculated the fraction of arches with different number of beads for each case (Figs. 3(b)–3(e)). Clearly, in the flat-bottom silo (Fig. 3(b)) the arches that clog a given outlet size are rather heterogeneous in the sense that they can be composed of different number of beads. On the contrary, for the $\beta = 80^\circ$ hopper (Fig. 3(e)), almost the only arches that develop for each outlet size are those where the number of beads is equal to the value obtained by rounding D/d upwards.

The results of Fig. 3 can be seen as if increasing the hopper angle leads to a screening of the arches that can be formed above the orifice. This spontaneous mechanism for selecting clogging arches allows us to study the probability of arch formation as a function of the number of beads in them, p_{cn} . In analogy with the definition of the probability of clogging (p_c) [29], p_{cn} is defined as the probability that an arch of n particles clogs the outlet. The outcomes for the different outlet sizes and hopper angles are shown in Fig. 4. Clearly, for a flat-bottom silo, the probabilities of forming arches of 3, 4, 5... particles show a smooth decreasing trend with D/d . Also, as expected from our findings of Fig. 3, in this geometry the contribution to the total probability of clogging for each D/d is shared among arches of different number of particles. Oppositely, in a $\beta = 80^\circ$ hopper, the clogging

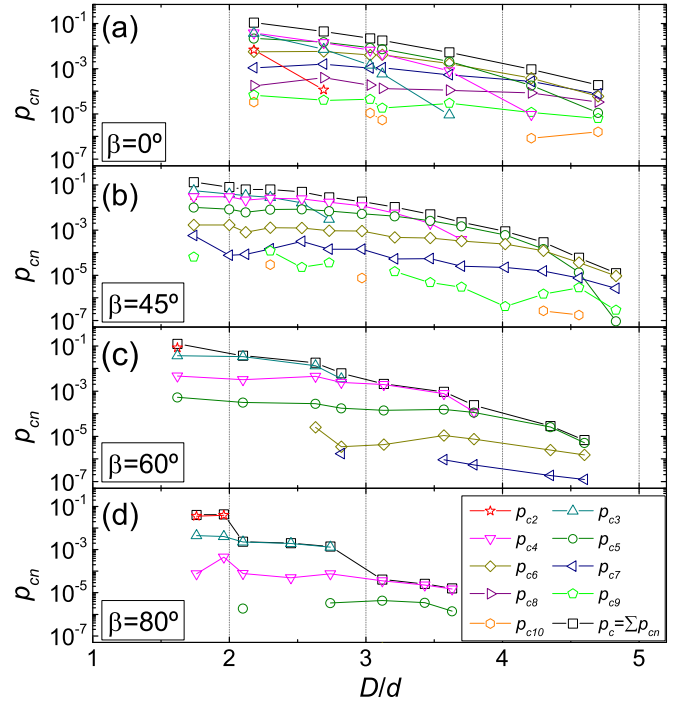


FIG. 4. Probability of clogging p_c versus the outlet size for the four hopper angles explored in this work. Empty squares account for the probability that the orifice gets clogged by any kind of arch whereas the other symbols correspond to p_{cn} , the probability that the orifice gets clogged by an arch of n particles. Note the logarithmic scale on the vertical axes.

probability practically coincides with p_{c2} for $D/d < 2$, p_{c3} for $2 < D/d < 3$, and p_{c4} when $3 < D/d < 4$. Interestingly, the values of p_{cn} remain rather constant for the whole range of D/d (yet a weak dependence is perceived). Again, this result evidences that only a small fraction of the arches that form in a flat-bottom silo is permitted when implementing the $\beta = 80^\circ$ hopper. This arch selection is clearly behind the increase of the mean avalanche size observed in Fig. 2 (as the number of allowed clogging arches is reduced) and the step-wise dependence of this parameter on D/d .

In order to unveil the reasons behind the hopper effect on clogging, we have analyzed the geometry of all the arches by looking at the vector angles, θ , that every two consecutive particles of the arch make with the horizontal. The probability density functions of θ obtained for the different outlet sizes and hopper angles are reported in Fig. 5. Undoubtedly, the hopper angle is the parameter that determines the distribution of θ whereas the outlet size has a negligible effect. The first salient feature of Fig. 5 is the existence of some peaks at values of θ that depend on the hopper angle (at $\theta = 60^\circ$ for $\beta = 0^\circ$, $\theta = 15^\circ$ for $\beta = 45^\circ$, and $\theta = 0^\circ$ for $\beta = 60^\circ$), a feature that might be related with crystallization effects. More importantly, we observe that the distributions become narrower as the hopper angle increases. In other words, the hopper geometry prevents the formation of arches with particle arrangements of very large $|\theta|$. This feature can be understood by a geometrical argument. Assuming frictionless particles (which can be experimentally approached using hydrogel spheres [10,30]) in a $\beta = 80^\circ$ hopper, the angle

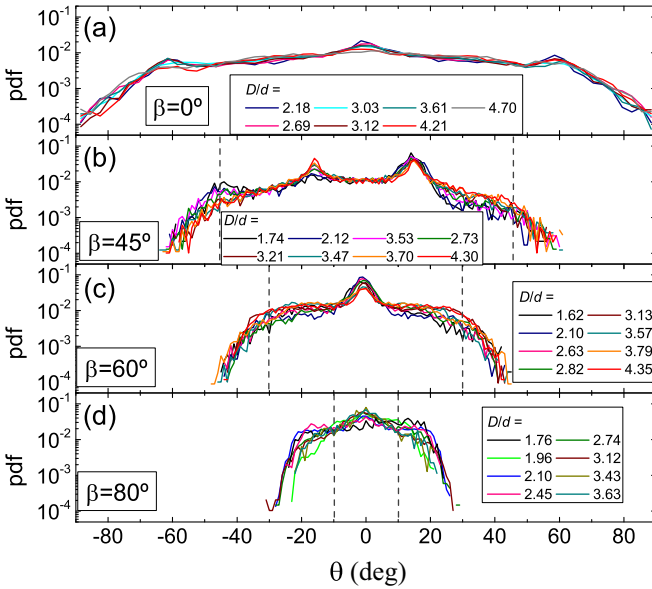


FIG. 5. Probability density functions (pdf) of the vector angle θ that every two consecutive particles make with the horizontal, as defined in Fig. 2(a). Results are presented for the four hopper angles investigated in this work and different outlet sizes as indicated in legends. Dashed lines indicate the limit values of θ that would be possible for frictionless grains. Note the logarithmic scale on the vertical axes.

θ_1 formed by the first two particles (starting from the left) would necessarily be smaller or equal to 10° ($90^\circ - \beta$). Otherwise, the leftmost particle of the arch would be hanging below the line that is perpendicular to the hopper and reaches the second particle. This arrangement is intrinsically unstable unless there is friction, and was called a defect in a previous work [28]. In the same way, if we want to prevent the existence of these defects in the arch, θ_2 (the angle formed by the second and third particle) has to fulfill the condition of being smaller or equal to θ_1 . This requirement was originally suggested in [12] to preserve the arch convexity in the proposed restricted random walk model. Therefore, considering the geometrical constraints introduced by the hopper boundaries on the angles that can subtend the particles in contact with them, we can rewrite the angular restriction in [12] as

$$(90^\circ - \beta) \geq \theta_1 \geq \theta_2 \geq \theta_3 \geq \dots \geq \theta_{n-1} \geq -(90^\circ - \beta). \quad (1)$$

Thus, the distributions of θ for an hypothetical frictionless granular sample should be restricted to values comprised between $90^\circ - \beta$ and $-(90^\circ - \beta)$; i.e., $10^\circ \geq \theta \geq -10^\circ$ for $\beta = 80^\circ$, $30^\circ \geq \theta \geq -30^\circ$ for $\beta = 60^\circ$, and $45^\circ \geq \theta \geq -45^\circ$ for $\beta = 45^\circ$. These limits (marked with vertical dashed lines in Fig. 5) are not strictly fulfilled in the experimental distributions, an issue that we attribute to the role of friction which allows the existence of defects (small deviations from arch convexity). Nevertheless, the presence of cutoffs in the pdf(θ) at values of θ that decrease when β increases, supports the validity of the proposed idea. In principle, the flat bottom silo should not lead to any restriction in the values of θ , but the angle of repose of the stagnant region that spontaneously

develops within the silo, might be behind the cutoffs appearing at around $\theta = \pm 60^\circ$. According to this speculation, the angle of the stagnant region should be around 30° .

Once we have understood the origin of the restriction of θ imposed by the hopper boundaries, we proceed to connect this feature with the ones reported in Figs. 2–4. Clearly, for a $\beta = 80^\circ$ hopper, the restriction of $10^\circ \geq \theta_i \geq -10^\circ$ implies that the only arches that can develop are practically flat. Indeed, the allowed arch spans (l) can be calculated for the hypothetical case of frictionless particles. For example, arches of three particles can only have a span ranging from $(1 + 2\cos(10^\circ))d$ (corresponding to an arch with $\theta_1 = 10^\circ$ and $\theta_2 = -10^\circ$) to $3d$ (corresponding to an arch with $\theta_1 = \theta_2 = 0^\circ$). The span range allowed for all cases can be generalized in terms of the number of particles in the arch n and the hopper angle β as

$$(1 + (n - 1) \cos(90^\circ - \beta))d \leq l < nd. \quad (2)$$

The arch span intervals given by Eq. (2) are shown as shaded regions in Fig. 6. Note that for a flat-bottom silo all spans are possible whereas for the $\beta = 80^\circ$ hopper, the spans allowed are confined to small regions near integer numbers. Although this reasoning is only valid for a frictionless case, the experimental distributions of spans reported in Fig. 6 for $\beta = 80^\circ$ reveal a nice agreement (yet, because of friction, the pdf's extend slightly beyond the shaded regions). When the hopper angle decreases, the ‘quantization’ of the spans weakens as the peaks (and shadowed regions) widen. Finally, for the flat-bottom silo, only some peaks at $l/d = 2$ and $l/d = 3$ are visible for small outlet sizes, a behavior that has been attributed to the different probability at which particle arrangements can take place for the case of two and three particles arches [18,28,31].

Therefore, from the results of Fig. 6 we can conclude that the geometrical restriction imposed by the hopper inclination in the angles between particles, leads to a reduction of the allowed arch spans that become almost discrete for very inclined hoppers. Clearly, this is the reason behind the step-like shape of the avalanche size dependence on the outlet size reported in Fig. 2. Let us illustrate this with an example for the $\beta = 80^\circ$ hopper case. Due to the span restriction obtained from Eq. (2), when $D/d \approx 3.3$ (as in the right picture of Fig. 1) arches cannot form at the lowest part of the hopper, because they would require the existence of θ values out of the range $10^\circ \leq \theta \leq -10^\circ$. Indeed, the only position within the hopper at which four-particles’ arches can develop is where the neck length is almost $4d$. And this happens for the whole range $3 < D/d \leq 4$, over which exactly the same kind of arches would develop independently on the value of D/d . As a result, we have a probability of forming a clogging arch of four particles that remains almost constant for $3 < D/d \leq 4$. Of course, for this range of aperture sizes, it is also possible (but more unlikely) to have an arch of five particles that must necessarily develop upwards within the hopper, at a height that corresponds to a neck length of almost $5d$.

The counterpart of the $\beta = 80^\circ$ hopper case is the flat-bottom silo. There, particles within the arches have not restriction of angles imposed by the walls. Hence, apart from the flat arches found for $\beta = 80^\circ$, many other shapes are possible. Indeed, it was previously shown that semicircular

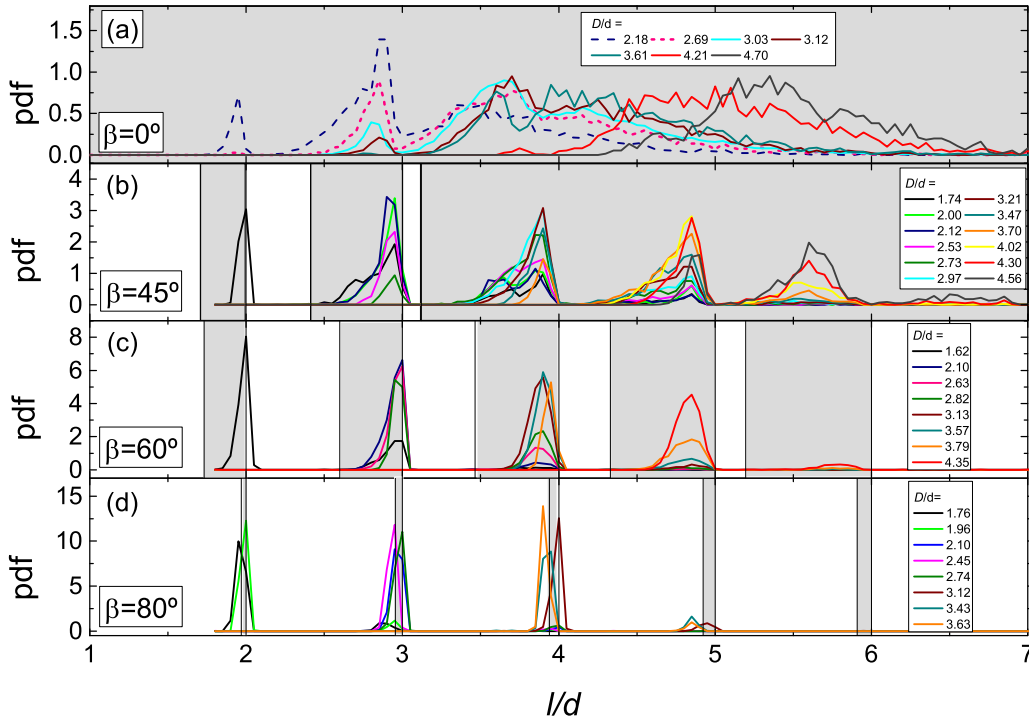


FIG. 6. Probability density functions of the arch spans l . Experimental results are presented for different hopper angles and outlet sizes as indicated in legends. The shadowed regions in each plot correspond to the only arch spans that would be possible for frictionless grains according to Eq. (2).

arches are predominant in a flat-bottom silo [28]. As a result, the probability that the flat-bottom silo gets clogged is the combination of many different probabilities of forming arches composed of different number of particles, and with a variety of shapes [31,32]. Therefore, the probability of clogging reduces smoothly with D/d (without sudden jumps) and the mean avalanche size grows in the same manner.

IV. CONCLUSIONS

In this work we have reported a new feature of clogging that has come to light by working with hoppers of different angles. In particular, we have discovered that the hopper walls introduce a geometrical restriction for the arches that can develop at the orifice. For very large hopper angles only flat arches are stable, an instance that has two important consequences:

(i) Clogging probability decreases when increasing the hopper angle as the number of allowed stable arches is reduced. This feature is especially visible for large outlet sizes where we have seen that the avalanche size increases in almost three orders of magnitude when comparing a $\beta = 80^\circ$ hopper with a flat bottomed silo. This behavior could also occur (perhaps to a lesser extent) in other systems of discrete particles flowing through a constriction (such as pedestrian, colloidal or active particles); therefore, our finding might be of practical importance as it could be implemented to reduce clogging in a wide variety of situations.

(ii) The dependence of clogging probability (or avalanche size) with the outlet size becomes discretized for very large hopper angles. As the only geometrically stable arches in a

$\beta = 80^\circ$ hopper are almost flat, there is a strong restriction in the allowed arch spans: only those values slightly below an integer number are possible. Therefore, the probability of clogging obtained with an outlet of $D/d = 3.1$ is similar than the one reached for $D/d = 3.9$.

The results reported in this work also show, in an indirect way, the relevance that the inter-particle friction has in the process of clogging; an effect which is enhanced as the hopper angle increases. This is reflected by the proportion of vector-angles (θ) among consecutive particles that do not fulfill the stability criteria for frictionless grains [as given in Eq. (1)] which is around 3%, 6%, and 33% for $\beta = 45^\circ$, $\beta = 60^\circ$, and $\beta = 80^\circ$, respectively. Indeed, we hypothesize that grains with an extremely high friction would minimize (or even suppress) the stepwise property of the avalanches, since it could suppress the stability criterion on the angle (as it already happened with v-shaped grooves in the seminal work of To *et al.* [12]).

Finally, let us mention that some of the reported findings—such as the step-like shape of the avalanche size versus D/d —could appear (or be magnified) due to the monodisperse nature of the granular sample. Indeed, the possible arch spans given by Eq. (2) for a polydisperse sample would be less restrictive than in the monodisperse case, as d takes many different values (and not only one). Nevertheless, we still expect that hopper geometries lead to clogging reduction for a polydisperse sample as the restriction imposed by the hopper in the angles between particles holds in this case. Also, other features such as the extrapolation to a three-dimensional case, or the effect of the particles' dynamics [33] (which could slightly vary in the range of $3 < D/d \leq 4$ leading to changes in the mean avalanche size) should be studied in the future.

ACKNOWLEDGMENTS

This work was funded by Ministerio de Economía y Competitividad (Spanish Government) through Project No. FIS2017-84631-P, MINECO/AEI/FEDER, UE. D.L. acknowledges Asociación de Amigos and D.G. acknowledges Ministerio de Economía y Competitividad (Spanish Government) for Grant No. BES-2015-074436.

-
- [1] G. A. Patterson, P. I. Fierens, F. Sangiuliano Jimka, P. G. König, A. Garcimartín, I. Zuriguel, L. A. Pugnaloni, and D. R. Parisi, *Phys. Rev. Lett.* **119**, 248301 (2017).
- [2] I. Zuriguel, D. R. Parisi, R. C. Hidalgo, A. Janda, P. A. Gago, J. P. Peralta, L. A. Pugnaloni, E. Clément, D. Maza, I. Pagonabarraga, and A. Garcimartín, *Sci. Rep.* **4**, 7324 (2014).
- [3] D. Helbing, I. Farkas, and T. Vicsek, *Nature* **407**, 487 (2000).
- [4] A. Garcimartín, D. R. Parisi, J. M. Pastor, C. Martín-Gómez, and I. Zuriguel, *J. Stat. Mech.- Theory Exp.* (2016) 043402.
- [5] E. Dressaire and A. Sauret, *Soft Matter* **13**, 37 (2017).
- [6] D. Genovese and J. Sprakel, *Soft Matter* **7**, 3889 (2011).
- [7] A. Marin, H. Lhuissier, M. Rossi, and C. J. Kähler, *Phys. Rev. E* **97**, 021102 (2018).
- [8] M. D. Haw, *Phys. Rev. Lett.* **92**, 185506 (2004).
- [9] D. Chen, K. W. Desmond, and E. R. Weeks, *Soft Matter* **8**, 10486 (2012).
- [10] X. Hong, M. Kohne, M. Morrell, H. Wang, and E. R. Weeks, *Phys. Rev. E* **96**, 062605 (2017).
- [11] C. Lozano, I. Zuriguel, and A. Garcimartín, *Phys. Rev. E* **91**, 062203 (2015).
- [12] K. To, P.-Y. Lai, and H. K. Pak, *Phys. Rev. Lett.* **86**, 71 (2001).
- [13] C. C. Thomas and D. J. Durian, *Phys. Rev. Lett.* **114**, 178001 (2015).
- [14] R. Arévalo and I. Zuriguel, *Soft Matter* **12**, 123 (2016).
- [15] A. Nicolas, A. Garcimartín, and I. Zuriguel, *Phys. Rev. Lett.* **120**, 198002 (2018).
- [16] A. Ashour, S. Wegner, T. Trittel, T. Börzsönyi, and R. Stannarius, *Soft Matter* **13**, 402 (2017).
- [17] S. Tewari, M. Dichter, and B. Chakraborty, *Soft Matter* **9**, 5016 (2013).
- [18] K. To and P.-Y. Lai, *Phys. Rev. E* **66**, 011308 (2002).
- [19] A. Longjas, C. Monterola, and C. Saloma, *J. Stat. Mech.* (2009) P05006.
- [20] L. Kondic, *Granular Matter* **16**, 235 (2014).
- [21] A. Anand, J. S. Curtis, C. R. Wassgren, B. C. Hancock, and W. R. Ketterhagen, *Chem. Eng. Sci.* **63**, 5821 (2008).
- [22] J. Choi, A. Kudrolli, and M. Z. Bazant, *J. Phys. Condens. Matter* **17**, S2533 (2005).
- [23] R. O. Uñac, A. M. Vidales, O. A. Benegas, and I. Ippolito, *Powder Technol.* **225**, 214 (2012).
- [24] M. Benyammine, P. Aussillous, and B. Dalloz-Dubrujeaud, *EPJ Web Conf.* **140**, 03043 (2017).
- [25] J. Wan, F. Wang, G. Yang, S. Zhang, M. Wang, P. Lin, and L. Yang, *Powder Technol.* **335**, 147 (2018).
- [26] S. Saraf and S. V. Franklin, *Phys. Rev. E* **83**, 030301 (2011).
- [27] A. Janda, I. Zuriguel, A. Garcimartín, L. A. Pugnaloni, and D. Maza, *Europhys. Lett.* **84**, 44002 (2008).
- [28] A. Garcimartín, I. Zuriguel, L. A. Pugnaloni, and A. Janda, *Phys. Rev. E* **82**, 031306 (2010).
- [29] p_c , the probability of clogging, is defined as $p_c = 1 - p$ where p is the probability that a particle passes through the outlet without forming a clog.
- [30] A. Ashour, T. Trittel, T. Börzsönyi, and R. Stannarius, *Phys. Rev. Fluids* **2**, 123302 (2017).
- [31] R. Arévalo, D. Maza, and L. A. Pugnaloni, *Phys. Rev. E* **74**, 021303 (2006).
- [32] L. A. Pugnaloni and G. C. Barker, *Physica A* **337**, 428 (2004).
- [33] D. Gella, I. Zuriguel, and D. Maza, *Phys. Rev. Lett.* **121**, 138001 (2018).